RAMAN AND IR STUDIES OF GRAPHITE INTERCALATES

S.A. SOLIN*

The James Franck Institute and the Department of Physics, The University of Chicago, Chicago, IL 60637, USA

Invited paper

The results of recent Raman scattering and infrared reflectance studies of donor and acceptor graphite intercalation compounds are reviewed along with corresponding measurements of pristine graphite. Newly calculated phonon dispersion curves of pristine graphite are discussed and related to the vibrational excitations of intercalation compounds. It is shown that proper sample characterization by X-ray and other techniques such as electron microprobe is crucial for correct interpretation of Raman and IR data. The nearest layer model for the intralayer vibrational excitations of graphite intercalation compounds is described in detail and justified by data on both donor and acceptor compounds. Intralayer intercalant modes in the $FeCl_3$ and Br_2 graphite systems are discussed and it is suggested that such modes are detectable as a result of resonance-Raman enhancement. The "zone-folding" and "disorder induced scattering" models for the Raman spectra of stage 1 alkali metal intercalation compounds are contrasted and the latter is shown to be more compatible with the observed spectra.

1. Introduction

Historically, the field of graphite intercalation compounds developed in such a way that the primary early emphasis was on sample preparation and synthesis [1]. Subsequently a good deal of research effort was devoted to the measurement of various physical and structural properties of intercalation compounds [2]. The structural measurements were on the whole crystallographic investigations aimed at determining atomic coordinates while the physical measurements focused upon bulk electrical and thermal properties [2]. It is only during the past four years that the lattice dynamical properties of graphite intercalation compounds have also been extensively studied. These studies were primarily conducted by Prof. Dresselhaus and her coworkers at MIT and by the author and his coworkers at the University of Chicago. The Chicago group also carried out extensive investigations of pristine graphite. These studies have provided a wealth of information both complimentary to and unattainable from more conventional investigations. In this paper I shall review the most significant results of the above described dynamical studies. The limited space available here necessitates a concise treatment of the subject which will, nevertheless, hopefully convey the information necessary to bring the interested reader up to date. In what follows I will assume that the reader has a basic knowledge of graphite intercalation compounds, i.e., that he/she is familiar with the phenomena of staging and the donor and acceptor classification scheme. Those requiring such background material are referred to reviews on the subject [2, 3].

Any discussion of lattice dynamics is facilitated by detailed if not complete knowledge of the structure of the dynamical system under consideration. Unfortunately such structural information is available for very few graphite intercalation compounds. Moreover there has been a recent explosion of knowledge on structural phase transitions in and the spatial dimensionality of graphite intercalates [4, 5] which further complicates a proper lattice dynamical treatment of any given compound. Thus, in this review I will concentrate upon compounds for which there is sufficient structural knowledge to justify a dynamical study.

2. Pristine graphite

In order to fully understand the dynamical properties of graphite intercalation compounds it is useful to consider the corresponding properties of pristine graphite. As is well known, graphite is the prototypical layer material the structure of which is shown in fig. 1 [6]. Note that the primitive cell of this homopolar material contains two layers and four atoms. Therefore graphite exhibits both a first order infrared and first order Raman response. A group theoretical analysis [7] of the graphite structure which has space group D_{6h}^4 indicates that the zone center optic modes can be decomposed into the following irreducible

* Present address: Department of Physics, Michigan State University, East Lansing, Michigan, USA.

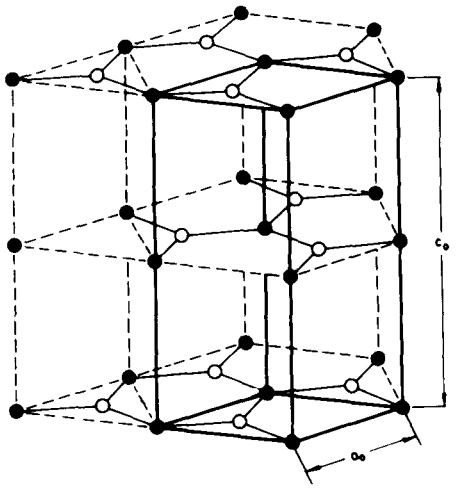

Fig. 1. Crystal structure of graphite, $a_0 = 2.45$ Å, $C_0 = 6.70$ Å.

representations:

$$\Gamma_{opt} = 2E_{2g} + E_{1u} + A_{2u} + 2B_{2g}. \quad (1)$$

Of these the E_{2g} modes are Raman active, the E_{1u} and A_{2u} modes are IR active and the B_{2g} modes are optically inactive. To test the group theoretical predictions of the number and activity of the optic modes recent Raman [8] and IR [9] studies have been carried out.

The results of those studies are shown in figs. 2a and 2b which indicate mode species, frequencies and atomic displacements. As can be seen from fig. 2a the Raman spectrum of highly oriented pyrolytic graphite [(HOPG)—see section 3.1] exhibits two E_{2g} modes as expected; one, labeled $E_{2g}^{(1)}$, is an in plane rigid layer shear mode which occurs at low frequency because the layers are rigidly displaced against the weak interlayer restoring force. The other, labeled $E_{2g}^{(2)}$, is also an in-plane mode but occurs at high frequency because the atoms are displaced against the strong nearest neighbor planar restoring forces.

The IR reflectance spectra of HOPG shown in fig. 2b contain, as expected, the in-plane E_{1u} mode [10] and the previously unobserved out of plane A_{2u} mode. As we shall see the latter adds a crucial constraint to any lattice dynamical model of the phonon dispersion curves of graphite.

The group theoretical approach outlined above is of course qualitative and does not account for the observed phonon frequencies or their dispersion properties. During the past two decades there have been numerous lattice

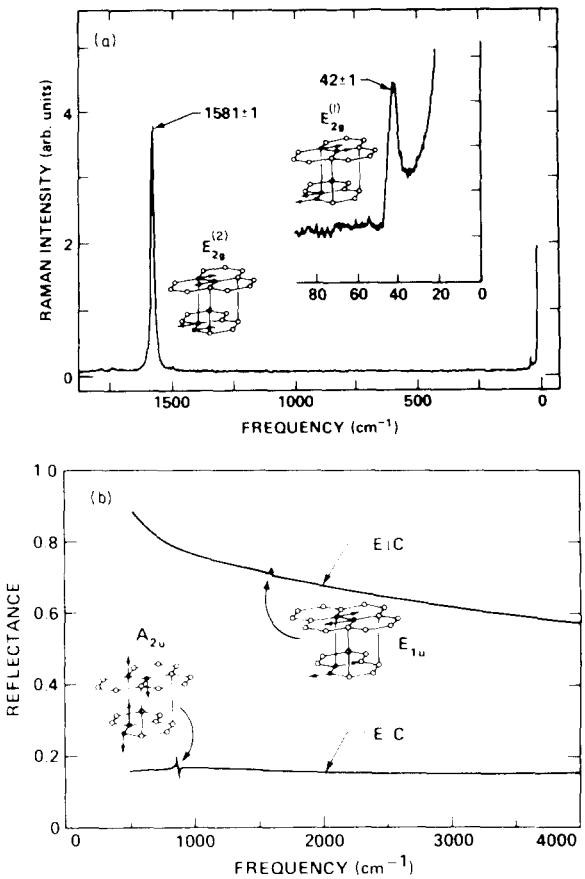

Fig. 2. (a) The Raman spectra obtained from a cleaved surface of graphite, and the atomic displacements of the Raman active E_{2g} modes. (b) The $E \perp C$ and $E \parallel C$ reflectance of graphite, and the atomic displacements of the IR active modes. The $E \perp c$, spectrum has been normalized for surface damage.

dynamics calculations of the phonon dispersion curves of graphite [11]. In each case the low frequency ($\omega \leq 500\,\text{cm}^{-1}$) neutron diffraction data [12] was fit; yet some of the models applied had mutually exclusive properties.

Nemanich and Solin [11] showed recently that the axially symmetric Born–von Karman model of Nicklow et al. [12] was the only one that could account for key features in the second order Raman spectrum of graphite. Yet even that model contained a serious deficiency: it predicted the A_{2u} mode to occur at $\approx 1400\,\text{cm}^{-1}$ instead of at $848\,\text{cm}^{-1}$, the observed value. However, Maeda et al. [13] have recently applied a modified Born–von Karman model which removes the constraint of axial symmetry. The results of their calculation are shown in fig. 3. The dispersion curves of fig. 3 provide the best fit

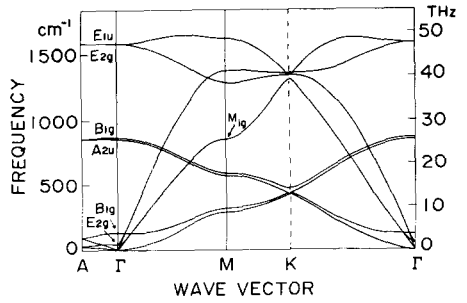

Fig. 3. Phonon dispersion curves for graphite in the [001], [100] and [110] direction. From ref. 13.

yet of all of the available data and in particular still exhibit *a* positive curvature at Γ of the uppermost branch. This feature is required by the second order Raman scattering data [11] and was previously present only in the axially symmetric model of Nicklow et al. [12]. Thus it appears now that not only the structure but also the lattice dynamics of pristine graphite is well understood. This knowledge will serve usefully as a basis for understanding corresponding properties of the intercalation compounds.

3. Intercalated graphite

3.1. Sample preparation and characterization

Literally hundreds of intercalation compounds of graphite have been prepared from powdered graphite and more recently from highly oriented pyrolytic graphite a material which is now almost universally used in the study of graphite intercalates. The recipes for such preparations are well accounted for in the chemical literature [14, 15]. However, for the physicist and/or physical chemist interested in studying the properties of intercalation compounds it is sample characterization that is of key importance. Therefore it is useful to dwell briefly on this subject which for some compounds is surprisingly controversial.

While there are several methods used to characterize intercalation compounds of graphite, e.g., chemical analysis, measurement of weight uptake [16] and dilitation [17], effusion studies [18], etc., most researchers in the field would agree that the most fundamental characterization technique is X-ray diffraction. Assume that the compound to be examined is a pure stage *n*. Here *n* is the *constant* number of carbon layers between *any* nearest pair of intercalant layers in a configuration that *regularly* repeats along the direction normal to the layer planes. Then by measuring the (001) X-ray diffraction pattern one can, in principle, establish the stage number *n* of a given compound [19]. A typical series of (001) X-ray measurements [20] for several stages in the graphite-$FeCl_3$ system is shown in fig. 4 which evidences the clear dependence of the diffraction pattern on stage.

However, Metz and coworkers [21] have shown recently that to properly characterize an

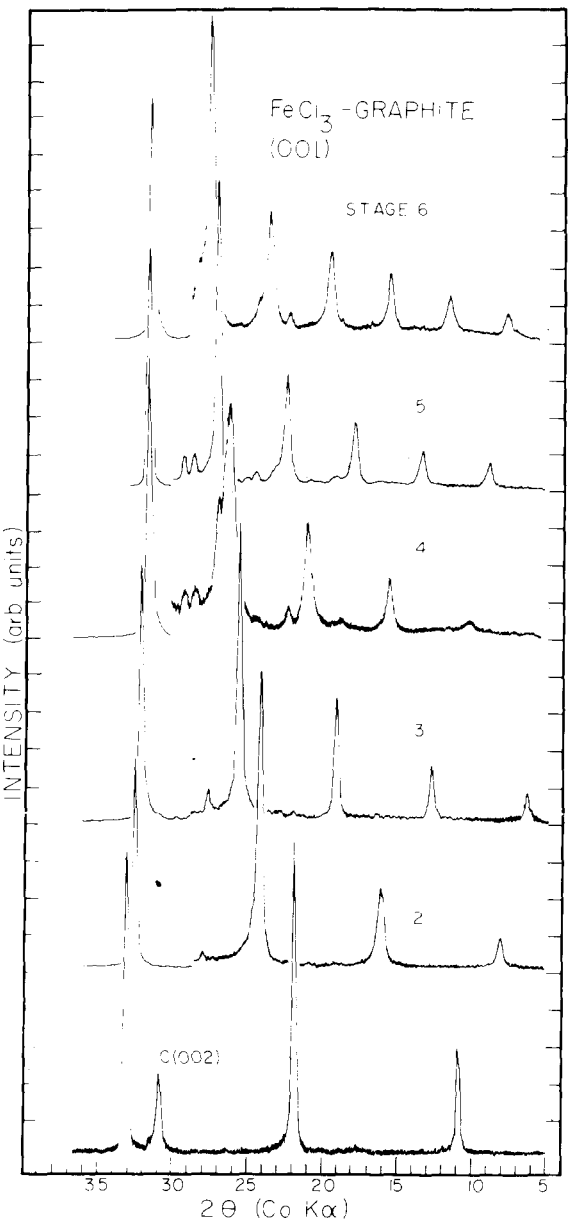

Fig. 4. [001] X-ray diffraction spectra of $FeCl_3$–graphite. The spectra were recorded at room temperature from single crystals with a CoKα source.

intercalation compound using (001) X-ray diffraction one must consider not only the number of reflections and their positions but also their spectral profile which indicates the degree of stacking disorder (see fig. 5).

Since this review is concerned with the dynamics of graphite intercalation compounds as probed by IR and Raman spectroscopy it is important to point out sample characterization problems which are unique to such measurements. First note that Raman measurements on intercalates are invariably carried out in the backscattering configuration [22] in which the incident photons excite only the surface region (≈1000 Å) of the sample. Similarly, IR reflectance measurement also probe only the sample surface. Moreover it is well known that the sample surface may differ drastically from the bulk in composition as well as other properties [23]. Therefore an X-ray diffraction study carried out with a "hard" source such as MoKα which penetrates deep into the sample (≈0.5 mm) may properly serve to characterize the bulk yet yield little information about the surface to which the optical probes are sensitive. But "hard" X-ray sources are most often employed to study intercalation compounds because such sources readily penetrate common encapsulating materials such as fused silica. Therefore, unless the optical probe is self-calibrating vis à vis sample characterization it is necessary to characterize optical samples with soft X-ray probes and/or other surface probes such as the electron microprobe.

3.2. Nearest layer model [22] of vibrational excitations

We now discuss the Raman response to the vibrational excitations of graphite intercalation compounds. There is general agreement [22, 24] on the interpretation of the high frequency ($\Delta\tilde{\nu} \geq 800\ \mathrm{cm}^{-1}$) Raman spectra of all compounds of stage 2 and higher measured to date. This is somewhat surprising since with few exceptions the in-plane structures of those compounds are unknown. In contrast the interpretation of the spectra of stage 1 compounds, and particularly those formed from the alkali metals, is still somewhat controversial even though the stage 1 alkali metal compounds are the most thoroughly characterized structurally.

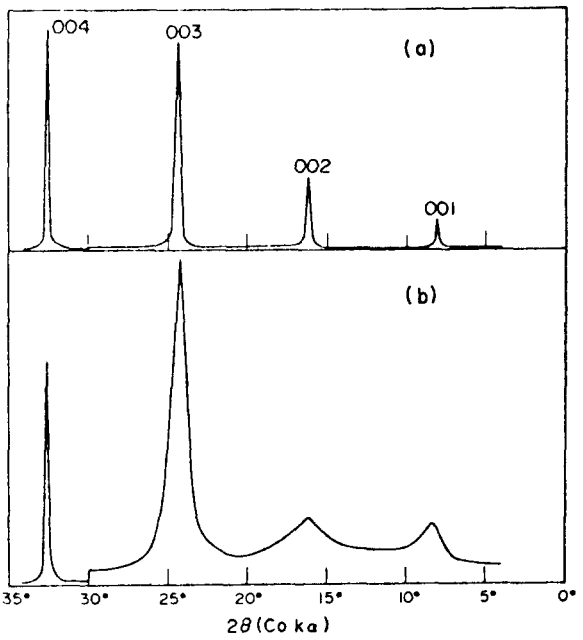

Fig. 5. Room temperature [001] X-ray diffraction spectra of (a) pure and (b) disordered stage 2 $FeCl_3$–graphite recorded with a CoKα source. From ref. 21.

Consider the possible nearest layer environments of the carbon layers in a pure stage n intercalation compound as depicted in fig. 6 [22]. In a stage 1 compound each carbon layer is bounded by a pair of intercalate layers (fig. 6A); there is only one nearest layer environment which we label type A. Similarly, in a stage 2 compound, each carbon layer is bounded by another carbon layer and an intercalate layer (fig. 6B); again there is only one nearest layer environment but it differs from that in a stage 1 compound and is labeled type B. In a stage n compound $n \geq 3$ there are just two types of

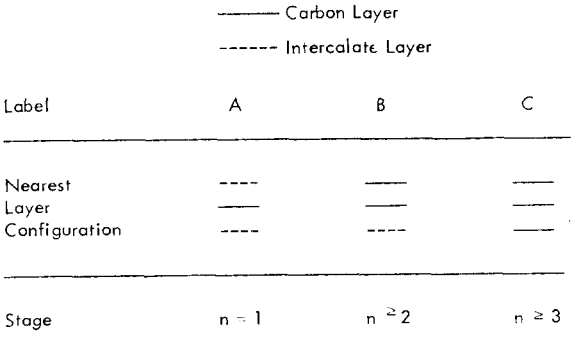

Fig. 6. Nearest layer configurations for carbon layers in graphite intercalation compounds.

nearest layer environments, one of type B which is identical to the environment in a stage 2 compound and one labeled type C in which a carbon layer is bounded by other carbon layers as in the case in pristine graphite [see fig. 6C].

Suppose now that the intralayer $E_{2g}^{(2)}$ mode of pristine graphite is sensitive to the nearest layer environment. Since the carbon hexagon layer structure is, to first order, undistorted in an intercalation compound [25], the atomic displacements corresponding to the $E_{2g}^{(2)}$ mode will also occur in an intercalated sample but the force constants which determine the mode frequency will depend on the nearest layer environment. Therefore the nearest layer model predicts that a pure stage 1 donor or acceptor compound should exhibit a single Raman band in the vicinity of but displaced in frequency from the $E_{2g}^{(2)}$ mode of pristine graphite. The same should be true for a stage 2 compound. However for stage 3 and higher stage compounds one expects to observe two high frequency Raman bands, one at the position of the $E_{2g}^{(2)}$ pristine graphite mode and one displaced in frequency. Furthermore the two bands which result respectively from type B and type C environments in stage n, $n \geq 3$ compounds should exchange intensity, the type C band at the position of the $E_{2g}^{(2)}$ pristine graphite mode becoming more intense with increasing stage number.

This latter point can be simply quantified by "counting" the number of layers having a particular nearest layer environment in a given stage n compound [23, 24]. From such a counting procedure one finds [23] that the relative integrated intensity ratio, R, of type B and type C derived Raman bands for stage $n \geq 2$ donor or acceptor compounds is

$$R \equiv \frac{I_C}{I_B} = \frac{n-2}{2}\frac{\sigma_C}{\sigma_B}. \tag{2}$$

Here I_B and I_C are, respectively, the intensities of the type B and type C Raman bands and $\sigma_C(\sigma_B)$ is the Raman cross section for scattering from an $E_{2g}^{(2)}$ type intralayer mode in a type C (type B) layer. Assume that σ_C/σ_B is stage independent which is equivalent to the assumption that the charge transfer to (from) the carbon layer is stage independent in a donor (acceptor) compound. Then R should be a linear function of n that intersects the n-axis at $n = 2$ and whose slope yields the Raman cross section ratio σ_C/σ_B.

The above described quantitative aspects of the nearest layer model were first tested by Solin [23] who studied stages 2 through 6 rubidium graphite. More recently the potassium graphite system has also been employed to test the model [26]. In fig. 7 are shown the room temperature Raman spectra of stages 2 through 6 potassium graphite. Similar spectra have also been reported for the rubidium graphite system [23]. The samples used to obtain the spectra of fig. 7 were properly characterized using the (001) X-ray reflections. Notice that as predicted the stage 2 compound exhibits a single high frequency line in the region of the $E_{2g}^{(2)}$ mode of pristine graphite while the higher stage compounds produce a doublet structure in this region.

By computer fitting each of the doublet spectra of fig. 7 with a pair of Lorentzians and correcting for instrumental broadening [26, 23] one can deduce accurate experimental values for I_C/I_B as a function of n. The stage dependence of I_C/I_B for both the potassium and rubidium intercalation systems is shown in fig. 8 which constitutes a definitive verification of the nearest layer model for the alkali donor compounds. But

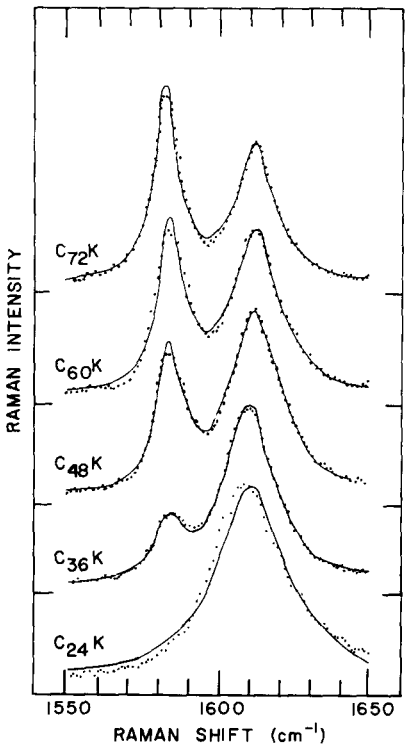

Fig. 7. Raman spectra of $C_{12n}K$ $n = 2 \ldots 6$. Lorentzian fit (—), Data (...).

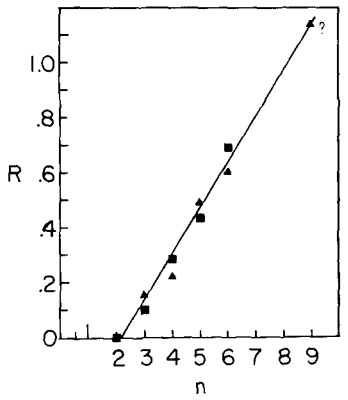

Fig. 8. The dependence of the intensity ratio R on n [see eq. (2)] for $C_{12n}Rb$ (▲) and $C_{12n}K$(■). The solid line is a linear least squares fit to the data.

fig. 8 also provides us with useful information on charge transfer and localization.

From the slope of the straight line fit to the data of fig. 8 we find that $\sigma_C/\sigma_B = 0.3 \pm 0.1$ for the potassium and rubidium intercalants. The vibrations which generate the B and C members of the Raman doublet at $\approx 1580\,cm^{-1}$ have essentially identical atomic displacements. The Raman cross sections σ_C/σ_B are determined from the polarizability which in turn depends on the atomic displacements and the amount of polarizable charge present in the layer. Therefore the ratio σ_C/σ_B is really a measure of the charge exchange and localization. If the carbon layer charge density measured along the c-axis was constant, as has been proposed on the basis of X-ray studies [27], then we expect $\sigma_C/\sigma_B = 1$. If for donors the B layers adjacent to the intercalant layer contain more charge than the C layers, we would expect to find $\sigma_B > \sigma_C$ and $\sigma_C/\sigma_B < 1$ as is observed in fig. 8. Thus the data in that figure indicate that the potassium and rubidium intercalation systems are electrically quite similar and that the charge exchanged to the carbon layers is not completely delocalized along the c-axis.

Eq. (1) should be applicable to acceptor compounds as well as donors. To date, the only acceptor system for which Raman studies of higher stage well characterized compounds have been carried out is the $FeCl_3$ system [20, 21, 29]. Underhill et al. [28] measured the high frequency Raman and IR spectra of stages 1, 2, 3, 4, 6 and 11 compounds which were characterized by X-ray measurements as "essentially single-staged". However a "hard" MoKα X-ray source was used and no attempt was made to assess the stage purity since the profiles of the X-ray reflections were not analyzed [see section 2.1]. The Raman results of Underhill et al. [28] are shown in fig. 9.

Solin and coworkers also studied the Raman spectra of compounds of $FeCl_3$–graphite in both the low frequency region [29] ($\Delta\tilde{\nu} < 350\,cm^{-1}$ to be discussed in section 3.3) and the high frequency region [20, 29]. Their samples which were prepared from single crystals were quantitatively characterized by examining the positions and profiles of the (001) reflections shown in fig. 4. On this basis they were found to be of high "purity". Nevertheless, depth dependent electron microprobe studies of the same samples indicated a high degree of spatial inhomogeneity along the c-axis direction [20] (resolution $\simeq$ 0.5 μ). The samples also exhibited large planar spatial inhomogeneities on their surfaces [20].

The data of fig. 9 were analyzed [28] using the two Lorentzian fit employed in the study of the potassium and rubidium compounds [23, 26]. I have used the parameters deduced from that analysis to plot R vs. n (see eq. (12)) as shown (open circles) in fig. 10. The notched line in that figure corresponds to a plot of eq. (2) with $\sigma_C/\sigma_B = 1$. No error bars are shown (open circles)

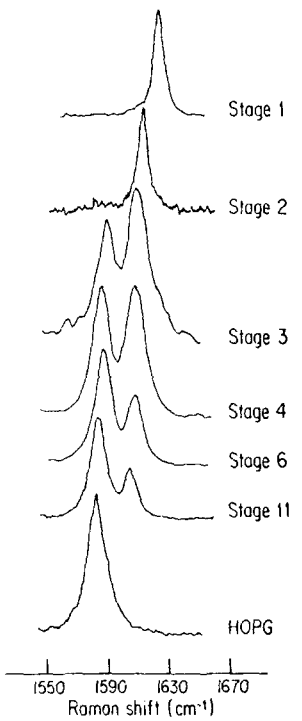

Fig. 9. The Raman spectra of stages 1, 2, 3, 4, 6 and 11 $FeCl_3$–graphite. From ref. 29.

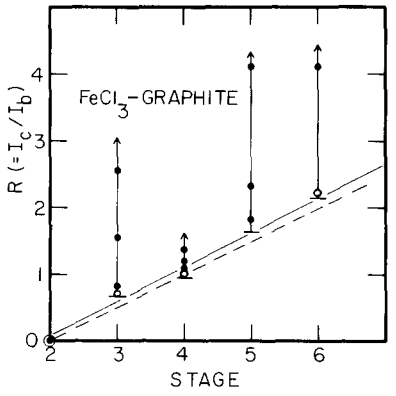

Fig. 10. The dependence of the intensity ratio R on n [see eq. (2)] for $FeCl_3$-graphite. ○—ref. 29, ●—ref. 20. The solid line is a least squares fit to the data of ref. 29. The notched line corresponds to $\sigma_C/\sigma_B = 1$ in eq. (1).

because insufficient information is available to properly determine them. It is reasonable, however, to assume that the data for the higher stage compounds, especially stage 11, are more uncertain than that for the lower stages. Data obtained from Raman measurements of the $FeCl_3$ system by Solin and coworkers [29] is also displayed in fig. 10 (solid circles). However, in this case the error bars are quite large as a result of the spatial inhomogeneities discussed above.

Qualitatively, the data of fig. 9 [see also fig. 3 of ref. 29] are perfectly consistent with the nearest layer model since the high frequency spectra of stages 1 and 2 yield singlets while for $n \geq 3$ a doublet is observed. Quantitatively, for $n < 11$ the open circles in fig. 10 can be reasonably fit by a straight line with a slope that yields the value $\sigma_C/\sigma_B = 1.16$. The closed circle data of fig. 10 are not inconsistent with that value but taken independently possess error bars which only permit the conclusion that $\sigma_C > \sigma_B$.

If, as in the case of donor compounds, we assume that the charge exchange is essentially stage independent, we would expect, on the basis of the nearest layer model, to find $\sigma_C > \sigma_B$ for all acceptor systems. This is expected because electronic charge is extracted *from* the type B layer in an acceptor compound thereby reducing σ_B relative to σ_C. Again, the magnitude of σ_C/σ_B indicates the degree of charge exchange and delocalization along the c-axis. The value of $\sigma_C/\sigma_B = 1.16$ determined from the data of Underhill et al. [28] is consistent with the known fact that the charge exchange is much smaller in the $FeCl_3$ system ($\leq 0.1e$/$FeCl_3$ unit) [30] than in the alkali metal system ($\approx 0.5e$/metal atom) [31]. Thus the polarizability of the type B layer is only slightly reduced relative to the type C layer which loses less charge and a σ_C/σ_B ratio close to 1 is obtained.

Underhill et al. [28] also measured the IR reflectance spectra of stages 1, 2, 3, 4, 6 and 11 graphite–$FeCl_3$. They found excellent qualitative agreement with a nearest layer model in which the E_{1u} IR active mode of pristine graphite plays the same role as the $E_{2g}^{(2)}$ mode does in Raman scattering. From an oscillator analysis of their Ir data they concluded that the fractional charge transfer per intercalant $FeCl_3$ unit was ≈ 0.75 for stages 1 and 2 and 0.95 for $n \geq 3$. They also concluded that 70% of the exchanged charge resided in the B layer while only 30% transferred to the C layers independent of stage. These results are in serious disagreement with other measurements and with the Raman analysis described above. For instance Mele and Ritsko [30] studied the core excitation electron loss spectrum of stage 1 $FeCl_3$ graphite and obtained a fractional charge transfer per intercalant of 0.07–0.12. Also the 70%–30% charge distribution would yield $\sigma_C/\sigma_B \approx 2.3$ in contrast to what is observed. It is possible that these discrepancies evolve in part from the equation of effective charge, e^*, which is determined in an oscillator analysis with the actual charge transfer.

3.3. *Intercalant modes*

The nearest layer model addresses only the perturbations to the 1580 cm^{-1} $E_{2g}^{(2)}$ mode of the pristine graphite host caused by intercalation. When the intercalant is a molecular or crystalline entity situated between the graphite planes one also expects to observe guest species modes. The first such observation was for the graphite bromine system [32, 33]. Whereas Br intercalates graphite as a molecular entity, $FeCl_3$, which crystallizes in a layer structure, enters graphite in the molecular vapor phase but crystallizes into layer domains having a lateral extent of ≈ 2000 Å [34, 35]. These conclusions were supported by a comparison of the polarized Raman spectra of pure crystalline $FeCl_3$ shown in fig. 11 with the polarized spectra of $FeCl_3$ graphite shown in fig. 12 [30].

Ferric chloride crystallizes in the BI_3 structure and has space group symmetry $C_{3i}^2(R\bar{3})$ with two

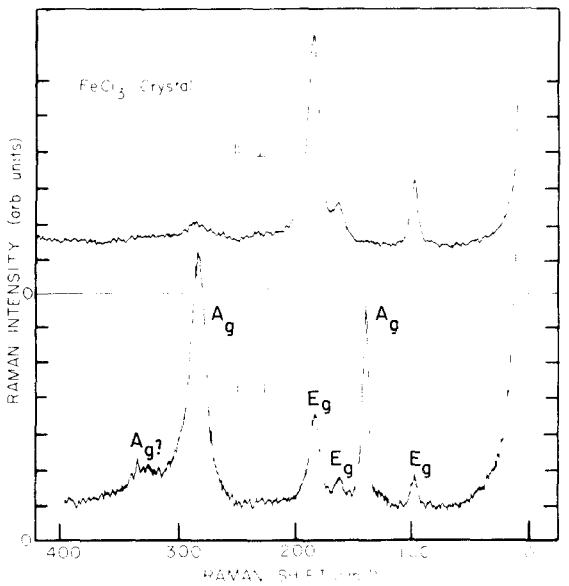

Fig. 11. Polarized Raman spectra of single crystal $FeCl_3$.

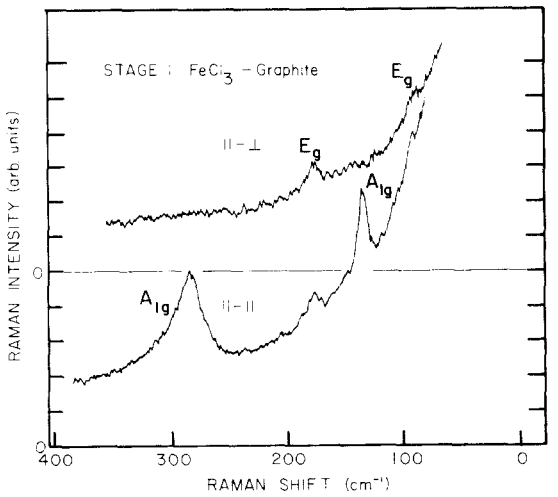

Fig. 12. Polarized Raman spectra of the intercalant intralayer modes of stage 1 $FeCl_3$–graphite.

molecular units in the rhombohedral primitive cell [36]. Its optic modes transform according to [29]

$$\Gamma_{\text{opt.}}^{\text{xtal.}} = 4A_g + 3A_u + 4E_g + 3E_u. \quad (3)$$

The "g" modes are Raman active and the "u" modes are IR active. Six of the eight Raman modes have been detected and are labeled in fig. 11. The $FeCl_3$ crystal is composed of layers the primitive cells of which also contain two $FeCl_3$ units. The layer symmetry is D_{3d} and its optic modes transform as [30]

$$\Gamma_{\text{opt.}}^{\text{layer}} = 2A_{1g} + 2A_{2g} + 4E_g + A_{1u} + 2A_{2u} + 3E_u. \quad (4)$$

Moreover the A_{1g} and A_{2g} layer modes correlate to the A_g modes of the crystal while the E_g layer modes correlate to the E_g crystal modes. The 2 A_{1g} modes can be detected at their expected positions in the Raman spectrum of stage 1 $FeCl_3$–graphite (see fig. 12) as can two of the 4 E_g modes. This is evidence for the layer structure of the $FeCl_3$ intercalant.

Since the Raman spectrum of pure stage 1 $FeCl_3$–graphite contains a single sharp line in the 1580 cm^{-1} region [29, 28] that line can be used to accurately characterize the sample surface being probed. The spectra of fig. 12 were obtained from a pure stage 1 region. Moreover the relative widths of the 139 cm^{-1} and 287 cm^{-1} modes in fig. 12 are significantly different from the corresponding features in the spectrum of crystalline $FeCl_3$ (fig. 11). Thus the spectra of fig. 12 do not arise from phase separated $FeCl_3$ on the sample surface.

Attempts to detect molecular internal modes in other acceptor systems, e.g., AsF_5 [37] have to date been unsuccessful. There is some evidence that the internal mode spectra of graphite $FeCl_3$, like those of graphite bromine may be resonance Raman enhanced [38]. It is possible then that intercalant modes which are not resonance-enhanced scatter too weakly to be detected.

We have, until now only discussed intercalant modes of acceptors. Naturally donor atoms (ions) can also generate additional Raman and IR excitations reflective of their interactions and structural arrangements. However, for the donors studied to date, e.g., the alkali metals, such excitations would occur at very low frequency [22, 24] and are experimentally inaccessible.

3.4. Stage-1 donor compounds

The stage 1 alkali intercalates C_8K, C_8Rb and C_8Cs are probably the most heavily studied of all graphite intercalation compounds. These compounds are crystalline at room temperature and their crystal structures are well established [39]. It is somewhat ironic then that conflicting interpretations of their Raman spectra have been presented by the MIT and Chicago groups while

their interpretations of the spectra of higher stage compounds, for which there is scant structural information are essentially identical.

The room temperature Raman spectrum of stage 1 C_8Cs [22, 40] is shown in fig. 13. The spectrum in fig. 13 is characteristic of the spectra of the other stage 1 compounds C_8K [22] and C_8Rb [23] and differs markedly from the Raman spectra of all other intercalation compounds studied to date. Unlike the spectra of higher stage donor compounds (see, e.g., fig. 7) and all acceptor compounds (see fig. 9 and fig. 3, ref. 29) the spectrum of fig. 13 consists of an intense continuous background on which is superposed a broad peak near 1500 cm^{-1} and a set of sharper features at $\approx$590 cm^{-1}.

There is general agreement [22, 24] on two features of the spectrum of fig. 13. The asymmetric peak at $\approx$1500 cm^{-1} results from a Fano interaction between a downshifted (i.e., pristine graphite) $E_{2g}^{(2)}$ like singlet (à la nearest layer model) and the continuum background. Moreover the continuum background for $\omega \leq$ 1000 cm^{-1} is phonon in origin [24, 40]. There are conflicting explanations [24, 40] of the 590 cm^{-1} feature and the origin of the phonon background.

Dresselhaus and coworkers attributed the 590 cm^{-1} feature which they observed as a doublet [24] to first order Raman scattering from excitations activated by the zone-folding or

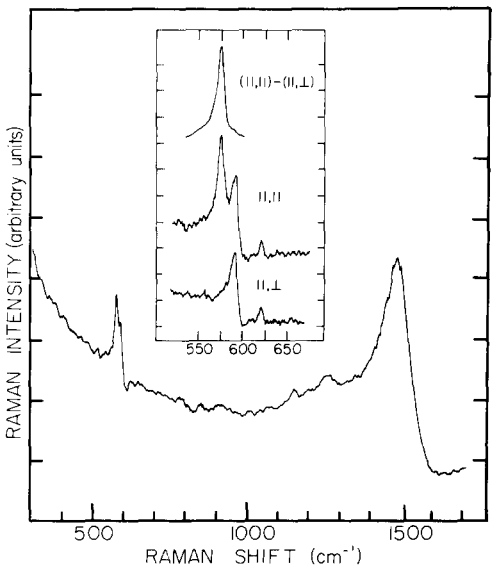

Fig. 13. Room temperature [polarized (insert)] Raman spectrum of stage 1 C_8Cs.

mapping of zone boundary M_{1g} modes into A_{1g} + E_g modes at the zone center. This mapping results from the enlargement of the graphite layer real space cell caused by the presence of intercalant atoms. The zone-folding model could account for the symmetry of two of the three observed lines at $\approx$590 cm^{-1} but when applied to the phonon dispersion curves of fig. 3 yields an energy of $\approx$840 cm^{-1} in serious disagreement with experiment. In the zone-folding model, the continuum scattering is attributed to multiphonon Raman scattering of low energy ($\leq$30 cm^{-1}) phonons.

In contrast Solin and coworkers [40] attribute the 590 cm^{-1} triplet and continuum to disorder induced scattering caused by stacking faults [41]. In that case the polarization properties, ordering and energies of the 590 cm^{-1} triplet members (see insert of fig. 13) are accurately accounted for. In particular the 590 cm^{-1} excitations correspond to the M point out of plane modes at 593 in the phonon dispersion curves of fig. 3 and provide strong quantitative support for the correctness of the calculations [13] from which those curves are deduced. By carefully measuring the temperature dependence of the continuum background in the Raman spectrum of C_8Cs Caswell and Solin were able to show definitely that the background was *single* phonon derived and could not be multiphonon in origin [40].

While the above described disorder induced scattering model accounts well for the Raman spectra of stage 1 heavy alkali intercalates its reliance on stacking faults as the source of disorder is still somewhat speculative. Careful X-ray diffraction and Raman measurements on the same stage 1 samples together with a quantitative analysis of the type and distribution of stacking faults will be useful for further substantiation of disorder induced scattering.

4. Conclusions

The study of the vibrational excitations of intercalation compounds, particularly their Raman spectra, is a fruitful endeavor for several reasons. The Raman technique in conjunction with the nearest layer model can be usefully employed to characterize local regions of spatially inhomogeneous low stage compounds. More significantly, by probing the vibrational excitations it is possible to ascertain details of charge

exchange and localization. Since the expected lattice vibrations of any substance are intimately related to its structure, the Raman and IR spectra can be used to identify and confirm certain structural features of intercalation compounds. Finally, the Raman and IR spectra should be very useful probes of the dynamics of structural order–disorder transitions that have recently been extensively studied in alkali graphites with X-ray diffraction [40–43].

It is a pleasure to acknowledge the crucial contributions of my present and former students, N. Caswell and R.J. Nemanich, respectively to the acquisition and analysis of much of the data discussed in this paper. I also gratefully acknowledge my other collaborators D. Guérard, W. Metz and G. Lucovsky. The research described herein which was performed at the University of Chicago was supported by several agencies including the DOE, the NSF and the AROD.

References

[1] R.C. Croft, Q. Rev. 14 (1960) 1.
[2] A.R. Ubbelohde and F.A. Lewis, Graphite and Its Crystal Compounds (Clarendon, Oxford, 1960).
[3] See, e.g., Mat. Sci. and Eng. 31 (1977) and references therein.
[4] R. Clarke, N. Caswell, S.A. Solin and P. Horn, this conference.
[5] N. Caswell, S.A. Solin, T.M. Hayes and S.J. Hunter, this conference.
[6] R.W.G. Wycoff, Crystal Structures, Vol. 1 (Oxford Univ. Press, London, 1962) p. 26.
[7] K.K. Mani and R. Ramani, Phys. Stat. Sol. B 61 (1974) 659.
[8] R.J. Nemanich, G. Lucovsky and S.A. Solin, in Proc. of the Intl. Conf. on Lattice Dynamics, M. Balkanski, ed. (Flammarion, Paris, 1978) p. 619.
[9] R.J. Nemanich, G. Lucovsky and S.A. Solin, Solid State Comm. 23 (1977) 117.
[10] L.J. Brillson, E. Burstein, A.A. Maradudin and T. Stark, in Physics of Semimetals and Narrow Gap Semiconductors, D.L. Carter and R.T. Bate, eds. (Pergamon, Oxford, 1971) p. 187.
[11] R.J. Nemanich and S.A. Solin, Solid State Comm. 23 (1977) 417 and references therein.
[12] R. Nicklow, N. Wakabayashi and H.G. Smith, Phys. Rev. B 5 (1971) 4951.
[13] M. Maeda, Y. Kuramoto and C. Hori, Proc. of the Phys. Soc. Japan, in press.
[14] M.S. Whittingham and L.B. Ebert, in Physics and Chemistry of Materials with Layered Structures, Vol. 6: Intercalation Compounds, F. Levy, ed. (Reidel, Dordrecht, 1977) and references therein.
[15] E. Stumpp, Mat. Sci. and Eng. 31 (1977) 53 and references therein.
[16] W. Metz and L. Siemsgluss, Mat. Sci. and Eng. 31 (1977) 119.
[17] G. Hooley, Mat. Sci. and Eng. 31 (1977) 17.
[18] F.J. Salzano, S. Aranson and A. Ingraham, J. Amer. Ceram. Soc. 51 (1968) 465.
[19] W. Rudorff and E. Schultz, Z. Anorg. Chem. 277 (1954) 156.
[20] N. Caswell, S.A. Solin and W. Metz, Bull. Am. Phys. Soc. 24 (1979) 375 and to be published.
[21] W. Metz and D. Holwein, Carbon 13 (1975) 87.
[22] R.J. Nemanich, S.A. Solin and D. Guérard, Phys. Rev. B 16 (1977) 2965.
[23] S.A. Solin, Mat. Sci. and Eng. 31 (1977) 153.
[24] M.S. Dresselhaus, G. Dresselhaus, P.C. Ecklund and D.D.L. Chung, Mat. Sci. and Eng. 31 (1977) 141.
[25] Some layer puckering may occur. See ref. 5, this conference.
[26] N. Caswell and S.A. Solin, Bull. Am. Phys. Soc. 23 (1978) 218 and to be published.
[27] D.E. Nixon and G.S. Parry, J. Phys. C 2 (1969) 1732.
[28] C. Underhill, S.Y. Leung, G. Dresselhaus and M.S. Dresselhaus, Solid State Comm. 29 (1979) 769.
[29] N. Caswell and S.A. Solin, Solid State Comm. 27 (1978) 961.
[30] E. Mele and J.J. Ritsko, Phys. Rev. Lett. 43 (1979) 68.
[31] I. Spain and D.J. Nagel, Mat. Sci. and Eng. 31 (1977) 183.
[32] J.J. Song, D.D.L. Chung, P.C. Ecklund and M.S. Dresselhaus, Solid State Comm. 20 (1976) 1111.
[33] P.C. Eklund, N. Kambe, G. Dresselhaus and M.S. Dresselhaus, Phys. Rev. B 18 (1978) 7069.
[34] J.M. Cowley and J.A. Ibers, Acta Cryst. 9 (1956) 421.
[35] K. Ohhaski and I. Tsujikawa, J. Phys. Soc. Japan 36 (1974) 422.
[36] R.W.G. Wycoff, Crystal Structures, Vol. II (Wiley, New York, 1964).
[37] N. Caswell and S.A. Solin, unpublished.
[38] N. Caswell, S.A. Solin and G.N. Papatheodorou, to be published.
[39] P. Lagrange, D. Guérard, M. El Makrini and A. Hérold, Comptes Rendu, in press and references therein.
[40] N. Caswell and S.A. Solin, Phys. Rev. in press.
[41] J.B. Hastings, W.D. Ellenson and J.E. Fischer, Phys. Rev. Lett. 42 (1979) 1552.
[42] H. Zabel, S.C. Moss, N. Caswell and S.A. Solin, Phys. Rev. Lett. in press.
[43] R. Clarke, N. Caswell, S.A. Solin and P. Horn, Phys. Rev. Lett. submitted.